ISSN: 1410-8917
Jurnal Kimia Sains & Aplikasi
e-ISSN: 2597-9914

Jurnal Kimia Sains dan Aplikasi 27 (9) (2024): 444-455

Jurnal Kimia Sains dan Aplikasi
Journal of Scientific and Applied Chemistry

Journal homepage: http://ejournal.undip.ac.id/index.php/ksa

Development of the Diffusive Gradient in Thin Film (DGT) Method with CaO/Biochar Binding Agent from Eggshells and Rice Straw Waste for Determining the Concentration of Phosphate

Asep Saefumillah [1,*], Siti Zahara [1]

[1] Department of Chemistry, Faculty of Sciences and Mathematics, University of Indonesia, Depok, Indonesia

* Corresponding author: asep.saefumillah@sci.ui.ac.id

https://doi.org/10.14710/jksa.27.9.444-455

Article Info

Article history:

Received: 05th July 2024
Revised: 16th September 2024
Accepted: 23rd September 2024
Online: 30th September 2024

Keywords:
DGT; CaO/biochar; eggshell; rice straw; phosphate; eutrophication

Abstract

Phosphorus, often found in the form of phosphate in the environment, especially aquatic environments, has been identified as the primary contaminant that causes algae blooms and eutrophication. Phosphate adsorption in the aquatic environment was carried out by comparing the adsorption capabilities of eggshell (CaO), rice straw (BC) and CaO/biochar materials at mass variations of 1:1, 1:2 and 2:1 from the use of eggshell and rice straw waste. Each material was synthesized using ball milling and pyrolysis methods. The adsorption isotherm and kinetics of the material are by the Langmuir adsorption isotherm and are pseudo-second-order (PSO) adsorption kinetics. The CaO/biochar 1:2 material shows the highest phosphate adsorption capacity at pH 12 with a contact time of 24 hours. CaO/biochar 1:2 was applied in the phosphate adsorption process using the Diffusive Gradient in Thin Film method as a binding agent, which acts as an adsorbent. The DGT technique is an in situ sample preparation technique for identifying the presence of phosphate, a labile species. The binding agent material was characterized using FTIR, XRD, and BJH-BET instruments. The success of synthesizing CaO/biochar 1:2 binding gel and ferrihydrite was demonstrated by the appearance of the same adsorption as the diffusive gel using FTIR. The CaO/biochar binding gel demonstrated that it is a better material compared to the ferrihydrite binding gel for phosphate adsorption, achieving C_{DGT} values of 10.1727 mg/L and 2.5959 mg/L at pH 5 and 3, respectively, with a phosphate concentration of 10 mg/L. These findings underscore the potential of CaO/biochar as a more effective material for phosphate removal applications.

1. Introduction

Phosphorus, commonly found in aquatic ecosystems as PO_4^{3-} (phosphate), is a crucial indicator of water fertility and pollution in rivers and seas. Phosphate levels significantly influence the balance of these ecosystems. Low phosphate levels (<0.01 mg P/L) inhibit plant and algae growth, causing oligotrophic conditions. High phosphate levels lead to excessive growth (eutrophic conditions), reducing dissolved oxygen and threatening aquatic ecosystem sustainability [1]. Therefore, the scientific and efficient management of phosphorus content in water is critical to maintaining ecological balance. However, phosphorus is a limited resource that cannot be naturally replenished. Over the next century, increasing demand for phosphate fertilizers will further deplete natural phosphorus reserves [2]. Hence, technology must be developed to prevent water eutrophication and address global phosphorus deficiency [3].

Previous research has developed and widely implemented chemical [4], biological [5], and crystallization [6] methods for controlling and treating phosphorus, particularly in aquatic environments. Among these methods, adsorption has proven to be an efficient and practical technology for preventing water eutrophication [7]. In the category of adsorbent materials, biochar has been recognized as an economical and environmentally friendly alternative due to its

optimal physical structure and potential to improve the chemical and physical properties of the environment [8]. While pure biochar efficiently adsorbs cations and organic pollutants, it has limited capacity for anionic pollutants like phosphate due to low metal cation content and ion loss during pyrolysis. Thus, biochar needs modification to enhance its phosphate adsorption capacity [9, 10, 11].

Eggshell waste, a type of biomass, is valuable as it contains crystalline calcite and protein fibers with calcium carbonate and a small amount of organic matter (about 6%). Eggshell waste is a valuable calcium source for producing modified biochar, which can absorb phosphorus and potentially serve as a phosphate fertilizer [12]. In a study conducted by Liu *et al.* [13], eggshell waste was used as a source of calcium and rice straw as a carbon source to develop a CaO/biochar composite. This composite was synthesized with varying weight ratios of eggshell waste to rice straw (2:1, 1:1, and 1:2). The results demonstrated that the composite effectively adsorbed phosphate in aquatic environments.

However, measuring phosphate presents challenges in sampling and storage, as improper handling can alter the sample's original composition, leading to potential analysis errors. Therefore, it is crucial to use a method that determines the number of phosphate species in situ to avoid errors in sample storage [14]. The diffusive gradient in thin films (DGT) technique is an effective in-situ and passive sampling method for measuring labile species in aquatic environments. It uses a hydrogel layer as a binding agent to accumulate analytes, calculated based on Fick's First Law. In this study, CaO/biochar was used as the binding agent, allowing for precise measurement of labile species concentrations and detailed information on analyte availability. The analyte concentration bound to DGT reflects its diffusion potential into aquatic biota, and DGT accurately measures phosphate or labile metal concentrations using diffusion coefficients without additional calibration [9].

2. Experimental

2.1. Materials

In the molybdenum blue method, a 100 g/L ascorbic acid solution (Merck) was prepared daily as the reducing agent. The mixed reagent solution was created by combining 30 mL of H_2SO_4 (1:1, $H_2O_2SO_4$) to acidify the reaction, 10 mL of a 130 g/L ammonium molybdate ($(NH_4)Mo_7O_{24}.4H_2O$) (Merck) solution to form a complex with phosphate, and 10 mL of a 3.5 g/L potassium antimony tartrate solution (Merck), which acted as a catalyst. This mixed reagent solution was stored at 4°C and remained stable for several months. Additionally, a phosphate stock solution of 500 mg P/L was prepared by dissolving pre-dried potassium dihydrogen phosphate (KH_2PO_4) (Merck) in distilled water for analysis.

The gel solution was prepared using the method by Zhang and Davison [9]. The polyacrylamide gel consisted of 40% acrylamide (Merck) and 0.3% cross-linker (N,N'-methylenebisacrylamide) (Merck) and was used as the diffusive gel layer. In a 10 mL beaker, 0.75 mL of N,N'-methylenebisacrylamide (MBA), 1.9 mL of 40% acrylamide, and 2.35 mL of distilled water are mixed. The mixture was stirred until homogeneous. Five milliliters of the gel solution were used for each synthesis of the diffusive and binding gels.

2.2. Synthesized of CaO/biochar

The straw was air-dried, chopped, ground using a mill, and sieved through a 50 mesh (0.25 mm) screen before use. Eggshells were washed thrice with distilled water and ground through a 50 mesh (0.25 mm) screen. A 20 g mixture of eggshell and straw powder was combined in weight ratios of 2:1, 1:1, and 1:2. After mixing, the mixture was finely ground through ball milling for 30 minutes at room temperature. Each sample was placed in a furnace, heated to 800°C at a heating rate of 5°C/min under a nitrogen atmosphere, and held at 800°C for 2 hours. The 800°C heat treatment temperature was chosen because eggshells begin to decompose at 650°C and decompose completely at 800°C [15].

After the furnace cooled to room temperature, the solid products, referred to as CaO/biochar 2:1, 1:1, and 1:2, were obtained. Following the ball milling and pyrolysis processes, the dry weights of the CaO/biochar 2:1, 1:1, and 1:2 materials were 8.7464 grams, 7.2244 grams, and 5.4095 grams, respectively. Additionally, the same treatment was applied to obtain the synthesized eggshell (CaO) and biochar from straw (BC) to compare the adsorption capacity of each material [13].

2.3. Characterization

The specific surface area (S_{BET}) and pore characteristics of CaO/biochar were measured using N_2 adsorption-desorption isotherms at 77 K with a Qudrasorb Evo system and calculated using the BJH method. XRD and FTIR analyses were conducted to study variations in the CaO/biochar material and the adsorbed phosphate. XRD patterns were recorded in the 2θ range of 1–90° using an Ultima IV diffractometer with Cu-Kα radiation (λ = 1.5418 Å). FTIR characterization was performed in the 4000–400 cm^{-1} range using a Shimadzu IR Prestige 21 instrument after the material was mixed with KBr powder and compressed into pellets.

2.4. Bulk Adsorption Experiments

All adsorption experiments were conducted in batches. A total of 0.05 grams of CaO/biochar was placed in a 100 mL polyethylene tube containing 50 mL of phosphorus solution at various concentrations. The tube was stirred at 220 rpm for a set time at pH 7 and 298 K and then filtered through a 0.45 µm filter. Phosphorus concentration was measured using the Molybdenum Blue UV-Vis Spectrophotometer method. The adsorption isotherm was studied by varying the initial phosphorus concentrations (0, 5, 10, 25, 50, 100, 150, and 200 mg/L) with an equilibrium time of 24 hours. Kinetics were evaluated by mixing 0.05 grams of CaO/biochar with a 10 mg/L phosphorus solution and stirring at 220 rpm, pH 7, and 298 K, with samples taken at various time intervals (15 to 1440 minutes).

To assess the impact of pH on phosphate adsorption, 50 mL of a 10 mg/L phosphorus solution was adjusted to initial pH values (3, 5, 7, 9, and 12), mixed with 0.05 grams of adsorbent, stirred at 25°C for 24 hours, filtered, and analyzed for final phosphorus concentration and pH. The same procedure was also applied to eggshell (CaO) and rice straw (BC) as control materials in this adsorption study.

2.5. Synthesis of Binding Gel from CaO/biochar and Ferrihydrite

A total of 0.5 grams of CaO/biochar was mixed with 5 mL of gel solution and sonicated for 15 minutes. After adding 35 µL of ammonium persulfate and 12.5 µL of N,N,N',N'-Tetramethylethylenediamine (TEMED), the mixture was stirred for 10 seconds, pipetted into a glass mold, and heated at 42°C for one hour to form a gel. The gel was soaked in demineralized water for 24 hours, with the water changed four times, and was then stored in demineralized water until use. The gel was cut into 2.5 cm discs and characterized using FTIR. The same process was applied to ferrihydrite for comparison, allowing for analysis and comparison of the gel's characteristics and properties with those of the reference materials [16].

2.6. Diffusive Gradients in Thin Film Applications

The DGT device was tested for deployment time, phosphate concentration, and pH effects. It was immersed in 30 mL of 10 ppm KH_2PO_4 solution for 2, 4, 8, 12, and 24 hours. For concentration variations, the device was soaked in 2, 4, 6, 8, and 10 ppm KH_2PO_4 solutions for 24 hours. In the pH tests, the device was immersed in 10 ppm KH_2PO_4 at pH levels of 3, 5, 7, 9, and 12 for 24 hours. The device was positioned at three-quarters of the solution height and secured with a non-absorbent strap. To measure the phosphate concentration, the gel was eluted with 1 N NaOH for 24 hours.

3. Results and Discussion

3.1. Synthesized of CaO/biochar

Equation 1 highlights calcium (Ca) as an effective metal for enhancing biochar's adsorption capacity in pollutant removal. During high-temperature pyrolysis, eggshell calcium carbonate decomposes into CaO and CO_2, with CO_2 as an activation agent that enlarges pore size. Incorporating eggshells into biochar also increases specific surface area and pore volume. In this study, eggshell waste provides calcium, while rice straw is the carbon source for biochar composites produced through ball milling and pyrolysis. The calcination process is represented by Equation 1.

$$CaCO_{3(s)} \xrightarrow{\text{calcination}} CaO_{(s)} + CO_{2(g)} \quad (1)$$

Ball milling involves shear forces that reduce particle size through collisions and friction using zirconia or steel balls in a rotating shell [17]. Besides powder material refinement, ball milling is also utilized to synthesize oxides or nanocomposites and optimize structure or phase compositions. Mechanically activated with ball milling has been proven to enhance material reactivity and distribute elements evenly within the space [18]. On the other hand, pyrolysis is a thermal decomposition method of organic materials at high temperatures without oxygen. The main advantage of pyrolysis is its ability to reduce exhaust gas emissions by up to 20 times. In this research, heating was performed at 800°C with a heating rate of 5°C/min under a N_2 atmosphere and maintained at 800°C for 2 hours [15].

3.2. Characterization of CaO/biochar

3.2.1. Fourier Transform Infrared Spectroscopy (FTIR)

Information about the vibration of functional groups on CaO and rice straw involved in the adsorption of adsorbate molecules is shown in Figure 1. Spectral IR analysis shows different peaks at 709, 879, and 3293 cm^{-1}. The intense peak for eggshell particles is observed at 1088 cm^{-1}, indicating the presence of C-O from amide and amine groups, and at a wavenumber of 1448 cm^{-1}, which is closely related to the presence of carbonate minerals in the eggshell matrix. The peak observed at 3293 cm^{-1} is due to hydroxyl (-OH) group stretching. Two peaks can be observed at 709 and 879 cm^{-1}, each indicating the presence of calcium carbonate ($CaCO_3$). This suggests that eggshells, as an adsorbent, can interact with phosphate in an aqueous solution due to carbonate groups in the spectrum. The band at 2879 cm^{-1} represents C-H vibrations, indicating the presence of an organic layer made of amino acids on the eggshell. The band at 1655 cm^{-1} is associated with stretching C=O and carbonyl (amide) groups [19].

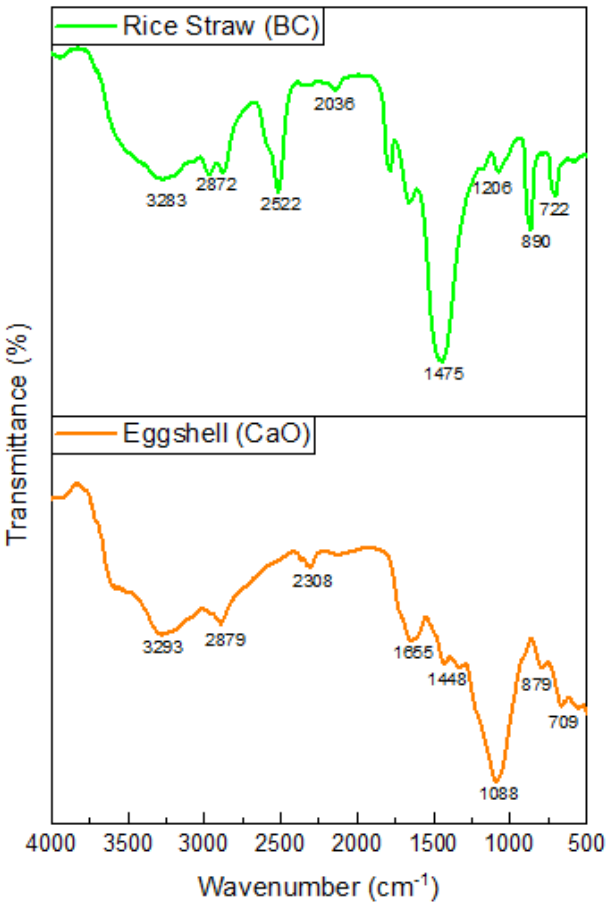

Figure 1. FTIR spectra of eggshell (CaO) and rice straw (BC)

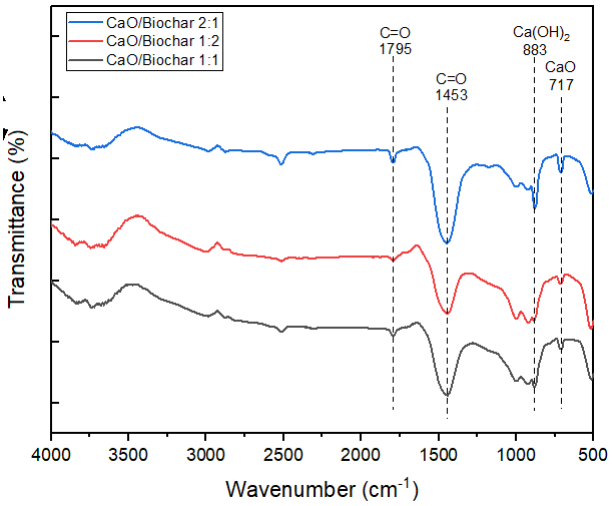

Figure 2. FTIR spectrum of CaO/biochar 1:1, CaO/biochar 1:2, and CaO/biochar 2:1

Meanwhile, the FTIR spectrum analysis of rice straw (BC). The broad and intense spectrum of rice straw (BC) observed at 3283 cm^{-1} indicates the presence of hydrogen-bonded (−O−H) functional groups in cellulose. Additionally, the band at 2872 cm^{-1} demonstrates the existence of aliphatic groups ($-CH_n$) stretching within the methyl and methylene groups of cellulose [20]. The vibration band around 1206 cm^{-1} is associated with the structural characteristics of hemicellulose. The adsorption band at 890 cm^{-1} indicates the presence of glycolic bonds (C−O−C) and C−O−C ring skeleton vibrations [21]. The adsorption peak near 2036 cm^{-1} shows aromatic C=C bonds, suggesting the presence of aromatic hydrocarbons such as benzene, phenol, ketones, and others. The adsorption peak for lignin near 1475 cm^{-1} is attributed to the skeleton vibration of C−C in aromatic rings. The adsorption peak around 722 cm^{-1} corresponds to the Si−O−Si group [22].

Figure 2 shows the FTIR spectrum of each CaO/biochar material with varying mass ratios of 1:1, 1:2, and 2:1, each weighing 20 grams. The FTIR spectra of each material show insignificant shifts in each variation. A weak intensity appears at a wavenumber of ~1700 cm^{-1}, indicating the presence of C=O bonds from carbonates. A strong intensity at a wavenumber of ~1400 cm^{-1} represents C=O bonds from CaO/biochar [23]. The C=O group at around 1800 cm^{-1} in the FTIR spectrum is due to the eggshells rich in calcium carbonate. During the high-temperature pyrolysis, the eggshells decompose into CaO and CO_2 [12]. The availability of functional groups (O-H, C-H, C-O, C=O, C=C, and COO-) enhances its ability to remove organic and inorganic pollutants from solutions. The formation of porosity, surface area, and functional groups depends on synthesis, activation methods, and biochar source [24]. The $Ca(OH)_2$ and CaO groups in the FTIR spectrum are shown at wavenumbers ~880 cm^{-1} and ~700 cm^{-1}, respectively. This indicates that calcium from the eggshells was successfully incorporated into the CaO/biochar 1:1, 1:2, and 2:1 composites in CaO and $Ca(OH)_2$. CaO is produced through the pyrolysis of calcium carbonate in the eggshells. Additionally, some CaO hydrates with H_2O in the environment to form $Ca(OH)_2$ [13, 25].

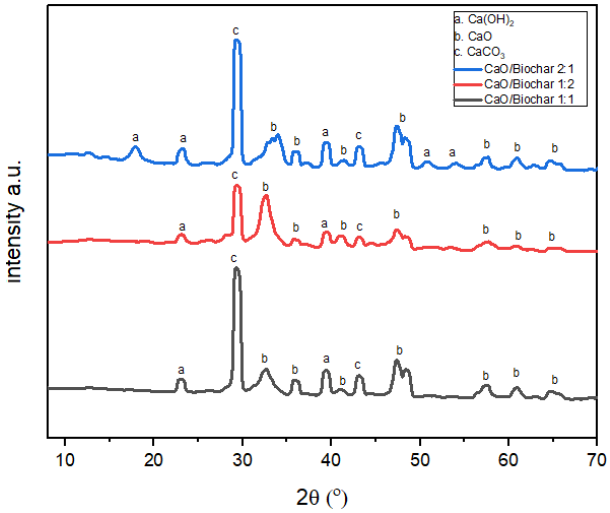

Figure 3. XRD pattern of CaO/biochar before adsorption

3.2.2. X-ray Diffraction (XRD)

As shown in Figure 3, the diffraction peaks at 2θ = 17.79°, 23.18°, 39.30°, and 50.89° for CaO/biochar before adsorption corresponds to the hexagonal phase of $Ca(OH)_2$ (PDF 44-1481). The diffraction peaks at 2θ = 33.85°, 47.34°, 53.94°, and 60.91° correspond to the Miller indices (111), (200), (220), and (311) of CaO, with a cubic structure (PDF-82-1691). Additionally, the characteristic peak at 29.26° corresponds to the rhombohedral phase of $CaCO_3$ (PDF 83-1762). At a temperature of 800°C for 2 hours, compounds such as $CaCO_3$, $Ca(OH)_2$, and CaO are formed, depending on the synthesis temperature. The formation of $CaCO_3$ always occurs with the synthesis method used in this study, as this calcium carbonate is an intermediate phase in obtaining CaO [26]. This indicates that eggshell calcium was successfully incorporated into the CaO/biochar material in $CaCO_3$, CaO, and $Ca(OH)_2$ forms. CaO is produced through the pyrolysis of calcium carbonate in the eggshells. Additionally, some CaO hydrates with H_2O in the environment, forming $Ca(OH)_2$. The intensity of $CaCO_3$ remains high, even comparable to CaO. Nonetheless, this material still has excellent adsorption capacity. This is because $CaCO_3$ also plays a role in adsorption [13].

3.2.3. Surface Area Analyzer

Figure 4 shows the adsorption-desorption isotherms and pore size distribution of CaO/biochar (1:1), CaO/biochar (1:2), and CaO/biochar (2:1) materials, indicating that these materials have a type IV isotherm according to International Union of Pure and Applied Chemistry (IUPAC). A type IV isotherm is characterized by an increase in adsorption volume at low to moderate relative pressures, followed by a significant rise at high pressures, indicating mesopores' presence. This structure suggests that the CaO/biochar materials have mesopores with diameters ranging from 2 to 50 nanometers. Based on characterization results using a surface area analyzer with the BET and BJH methods, the pore diameter of each CaO/biochar 1:1, 1:2, and 2:1 material is approximately ~3.87 nm, with no significant differences in pore size, indicating that CaO/biochar has a mesoporous type with pore sizes between 2-50 nm [12].

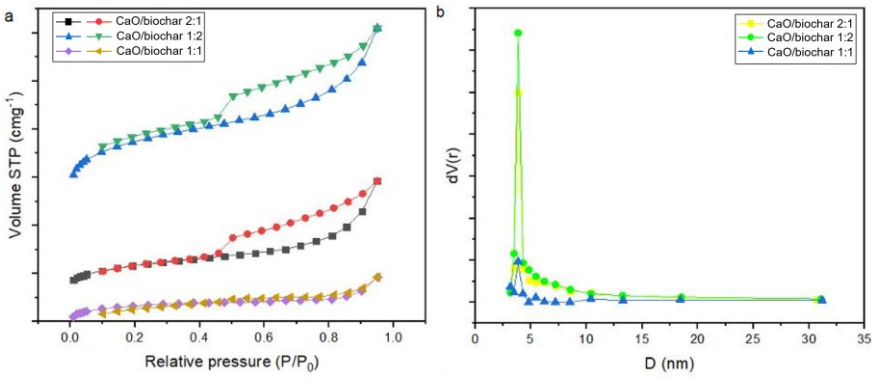

Figure 4. (a) Adsorption-desorption isotherms and (b) pore size distribution of CaO/biochar (1:1), CaO/biochar (1:2), and CaO/biochar (2:1) materials

Table 1. Surface area and pore diameter of CaO/biochar (1:1), CaO/biochar (1:2), and CaO/biochar (2:1) adsorbents

Material	S_{BET} (m^2/g)	Pore diameter (nm)
CaO/biochar (1:2)	88.77189	3.87
CaO/biochar (1:1)	40.25914	3.87
CaO/biochar (2:1)	24.86851	3.86

Table 1 shows that the CaO/biochar mixture with a 1:2 ratio has the highest specific surface area (S_{BET}) of 88.77189 m^2/g, while the CaO/biochar 2:1 mixture has the lowest S_{BET} of 24.86851 m^2/g. This difference can be explained by the varying ratios of calcium oxide (CaO) and biochar, where a higher proportion of biochar in the 1:2 ratio contributes to a more extensive porous network, thus increasing the specific surface area. During the pyrolysis process, calcium carbonate in eggshells decomposes into CaO and CO_2, with CO_2 acting as an activation agent that promotes the development of a porous structure within the biochar matrix [12]. Consequently, CaO/biochar materials have higher specific surface areas than pure biochar derived from rice straw, as Liu *et al.* [13] reported. However, the lower specific surface area observed in the 2:1 ratio is attributed to agglomeration on the material's surface. When there is a higher concentration of CaO, the particles tend to clump together, reducing the available active surface area and hindering optimal pore development.

Despite these changes in surface area, the pore size remains stable, with values around 3.87 nm for both the 1:2 and 1:1 ratios and a slight decrease to 3.86 nm for the 2:1 ratio. This stability in pore size can be explained by the fact that CO_2 activation primarily affects the overall porosity rather than the pore diameter. Although CO_2 increases the number of small pores, it does not significantly alter the existing pore sizes. Studies, such as Khine *et al.* [27], have confirmed that while CO_2 activation enhances specific surface area, its effect on pore size is limited. Thus, while the CaO/biochar ratio significantly impacts the particular surface area, the pore diameter remains unaffected mainly due to the limitations of CO_2 activation mechanisms and the influence of agglomeration on the pore structure. This highlights the importance of balancing CaO and biochar content to optimize performance in adsorption applications [13, 27].

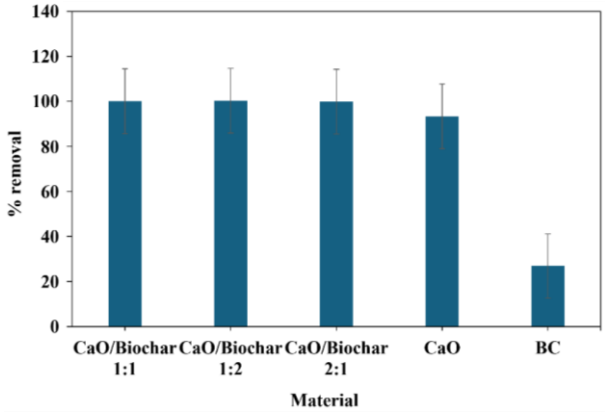

Figure 5. %removal in various materials: CaO/biochar, eggshell (CaO), and rice straw (BC)

3.3. The Effect of CaO/biochar Material Variations (1:1, 1:2, and 2:1), ES, and BC on Phosphate Adsorption

The observed high phosphate removal efficiency across different CaO/biochar ratios—2:1, 1:1, and 1:2—despite variations in specific surface area, is primarily attributed to the formation of hydroxyapatite (HAP) during the adsorption process. Figure 5 shows that the phosphate removal percentage for CaO/biochar with a 2:1 mass ratio is 99.92%, which is not significantly different from the 100.31% removal observed for both CaO/biochar 1:1 and CaO/biochar 1:2. This high removal efficiency can be attributed to the increased specific surface area and calcium content derived from the $CaCO_3$ in the eggshells incorporated into the rice straw during the CaO/biochar synthesis. The reaction of CaO with phosphate and hydroxide ions results in the formation of hydroxyapatite, significantly contributing to the high adsorption capacity.

$$5Ca^{2+} + 3PO_4^{3-} + OH^- \rightarrow Ca_5(PO_4)_3(OH)\downarrow \quad (2)$$

Despite the differences in the specific surface area among the CaO/biochar ratios, the high removal percentages indicate that the presence of CaO in the composite significantly enhances phosphate adsorption through chemical precipitation. The increase in specific surface area from the CaO/biochar composites facilitates more effective interactions with phosphates, but the overall high removal efficiency is primarily driven by the formation of hydroxyapatite. In contrast, individual components such as CaO from eggshells or biochar from

rice straw exhibit lower phosphate removal capacities (93.37% and 26.86%, respectively) due to the lack of chemical reactions with phosphates. The biochar from rice straw relies on physical adsorption within its pores, which is less effective compared to the chemical precipitation achieved with the CaO/biochar composite. Overall, the observed high efficiency in phosphate removal, regardless of specific surface area differences, highlights the crucial role of chemical reactions, particularly hydroxyapatite formation, in achieving effective phosphate adsorption [13, 24].

The FTIR spectrum of CaO/biochar shown in Figure 6 before and after phosphate adsorption at a wavenumber of ~1060 cm^{-1} represents asymmetric P-O vibrations, where the bond intensity significantly increases after the phosphate adsorption process. At a wavenumber of ~579 cm^{-1}, vibrations for P-O bonds also appear, proving that adsorption occurred on the CaO/biochar material with ratios of 1:1, 1:2, and 2:1 [28]. Compared to before adsorption, the FTIR spectrum of CaO/biochar after adsorption shows significant changes in peak characteristics, and the -OH stretching vibration band appears at ~3700 cm^{-1}. However, the -OH peak disappears after phosphate adsorption, indicating that the -OH group is involved in the phosphate removal [13].

After phosphate adsorption, the diffraction peaks of $Ca(OH)_2$ and CaO showed a significant reduction. The diffraction peaks at $2\theta = 25.63°, 32.46°, 39.28°$, and $46.97°$ indicate the presence of $Ca_5(PO_4)_3(OH)$, according to (PDF#76-0571), resulting from the reaction between Ca^{2+} and OH^- ions from $CaCO_3$, CaO, and $Ca(OH)_2$ with phosphate, as shown in Figure 7. Based on the characterization and analysis conducted, it can be concluded that the main adsorption mechanism for CaO/biochar with phosphate involves the combination of Ca^{2+} and OH^- ions with phosphate to form hydroxyapatite $Ca_5(PO_4)_3(OH)$ or (HAP), which explains the high adsorption capacity. The reaction was illustrated by Equations (3) to (5).

$$5Ca^{2+} + 3PO_4^{3-} + OH^- \rightarrow Ca_5(PO_4)_3(OH)\downarrow \quad (3)$$

$$5Ca^{2+} + 3HPO_4^{2-} + 4OH^- \rightarrow Ca_5(PO_4)_3(OH)\downarrow + 3H_2O \quad (4)$$

$$5Ca^{2+} + 3H_2PO_4^{-} + 7OH^- \rightarrow Ca_5(PO_4)_3(OH)\downarrow + 6H_2O \quad (5)$$

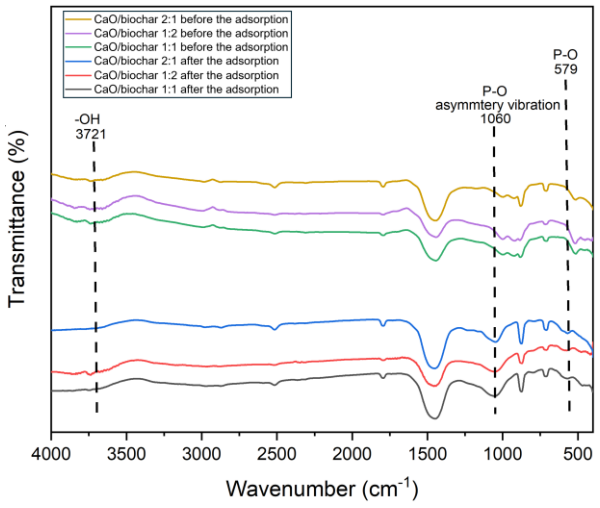

Figure 6. FTIR spectra before and after adsorption

In the phosphate adsorption process using CaO/biochar, both CaO, $Ca(OH)_2$ and $CaCO_3$ play crucial roles. CaO, when interacting with water, hydrolyzes to produce calcium ions (Ca^{2+}) and hydroxide ions (OH^-). These calcium ions then interact with phosphate ions (PO_4^{3-}) in the solution to form the hydroxyapatite complex ($Ca_5(PO_4)_3(OH)$). Meanwhile, $CaCO_3$, which may not be completely converted into CaO during synthesis, also contributes to adsorption. $CaCO_3$ partially dissolves in water to produce calcium ions (Ca^{2+}) and carbonate ions (CO_3^{2-}). The carbonate ions can further react with water to generate HCO_3^- and OH^-.

In contrast, the carbonate ions reacting with water to produce OH^- are important for the formation of hydroxyapatite ($Ca_5(PO_4)_3(OH)$). Additionally, carbonate and bicarbonate ions (HCO_3^-) act as pH buffers, maintaining optimal conditions for ($Ca_5(PO_4)_3(OH)$ formation. The Ca^{2+} produced from $CaCO_3$ interact with phosphate ions to form the $Ca_5(PO_4)_3(OH)$ complex. Thus, the significant presence of $CaCO_3$ in the material does not hinder the adsorption process but rather enhances the total adsorption capacity by providing more calcium ions that can bond with phosphate ions.

Therefore, even though the intensity of $CaCO_3$ in the XRD spectrum remains high, the adsorption capacity of the material remains excellent because both components, CaO and $CaCO_3$, work together to capture and hold phosphate ions through the formation of the hydroxyapatite ($Ca_5(PO_4)_3(OH)$) complex. Hydroxyapatite, with its stable crystal structure capable of effectively retaining phosphate, improves the overall adsorption capacity of the material [13, 26]. Moreover, the optimal pH for the study was 12, as the increased hydroxide ion concentration at this pH creates an ideal environment for hydroxyapatite formation, which maximizes phosphate removal. The buffering action of carbonate and bicarbonate ions helps maintain this pH, ensuring an efficient adsorption process. While the adsorption capacity did not vary significantly across a wide pH range, this demonstrates that phosphate adsorption can occur effectively from acidic to basic conditions, highlighting the material's versatility.

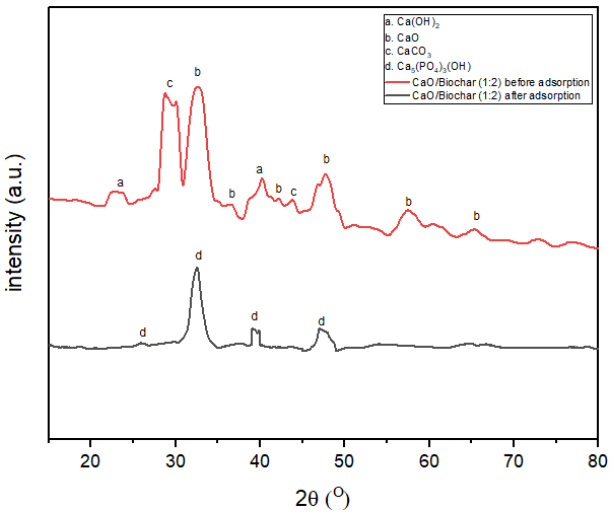

Figure 7. XRD pattern of CaO/biochar 1:2 after adsorption

Table 1. Table of adsorption isotherm test parameters

Adsorbent	Langmuir			Freundlich		
	Q_m	K	R^2	1/n	Kf	R^2
CaO/biochar 1:1	3.115265	0.10000	0.9905	-1.4777	1.106369	0.8373
CaO/biochar 1:2	0.925583	0.142817	0.9351	-0.4857	2.380126	0.5599
CaO/biochar 2:1	-0.12513	-0.11093	0.9961	1.0837	1.797629	0.8108

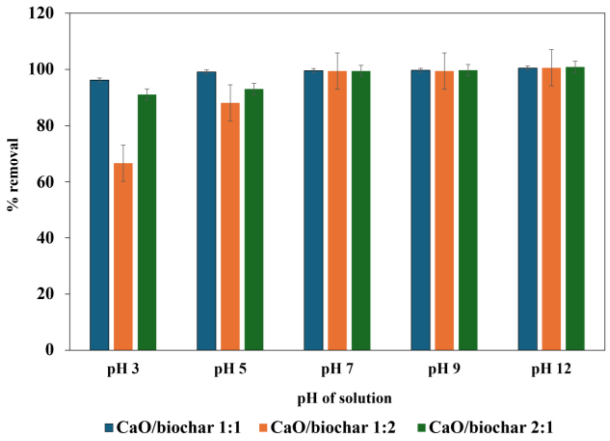

Figure 8. %removal of phosphate adsorption on CaO/biochar 1:1, 1:2, and 2:1

3.4. The Effect of pH on Phosphate Adsorption with CaO/biochar (1:1, 1:2, and 2:1)

Figure 8 illustrates the adsorption efficiency of phosphate using CaO/biochar (CaO/biochar) at different mass ratios (1:1, 1:2, and 2:1) over a range of pH values. The figure indicates that phosphate removal efficiency remains consistently high across most pH levels, particularly from pH 5 to 12, suggesting that the adsorbent is effective across various conditions [13]. However, at pH 3, adsorption capacity is significantly reduced across all mass ratios. This decline at lower pH levels can be attributed to increased competition between H^+ ions and phosphate ions for active adsorption sites.

In acidic environments, excess H^+ ions can inhibit the formation of calcium-phosphate complexes, leading to reduced adsorption. Phosphate removal efficiency improves at higher pH values, particularly at pH 12. This can be explained by the increase in OH^-, which enhances the negative surface charge of the adsorbent, promoting the electrostatic attraction of phosphate species. Additionally, as the pH increases, the dominant phosphate species shifts from $H_2PO_4^-$ (in acidic to neutral pH) to HPO_4^{2-} and PO_4^{3-} at higher pH values. The higher charge density of PO_4^{3-} at pH levels above 12.33 leads to stronger interactions with CaO, resulting in improved adsorption performance [29].

The study emphasizes that the ionization equilibrium of phosphate species controls phosphate adsorption. At pH 2.13–7.20, $H_2PO_4^-$ is the dominant species, while HPO_4^{2-} prevails between pH 7.20 and 12.33. Above pH 12.33, PO_4^{3-} becomes the primary species. The results show that CaO/biochar adsorbs phosphate most effectively when PO_4^{3-} is dominant, as it interacts more strongly with the adsorbent surface. Lower adsorption capacities for $H_2PO_4^-$ and HPO_4^{2-} are attributed to the presence of H^+ ions, which interfere with the complexation of calcium and phosphate. These findings suggest that CaO/biochar is a highly effective adsorbent for phosphate removal across a wide pH range, with the best performance in more alkaline conditions, making it a promising solution for treating phosphate-contaminated water in environmental applications [30, 31].

3.5. Isothermal Adsorption Experiment

The adsorption isotherm study of phosphate ions was conducted at a phosphate concentration of 10 mg/L with concentration variations of 2, 6, 8, 10, 12, 15, 20, and 25 ppm over 24 hours. All adsorption processes were performed at room temperature using each material variation of CaO/biochar 1:1, 1:2, and 2:1. The adsorption isotherm test is shown in Figure 9 and Table 1. The experimental data for CaO/biochar 1:1, 1:2, and 2:1 fit the Langmuir model ($R^2 > 0.9900$) better than the Freundlich model, indicating that the CaO/biochar adsorption process is monolayer adsorption with a homogeneous surface. The phosphorus adsorption process on other calcium-rich phosphate adsorbents, such as calcium-rich sepiolite [29], Ca-modified sludge [15], and calcium powder biochar [32], also fits the Langmuir model. CaO/biochar exhibits significantly higher phosphate adsorption performance due to the increased specific surface area and Ca species load due to the incorporation of $CaCO_3$ from eggshells into rice straw during the material synthesis process [13].

3.6. Adsorption Kinetics Experiment

The phosphate adsorption kinetics study using CaO/biochar was conducted over a period of 15–2880 minutes for different material ratios (1:1, 1:2, and 2:1) at room temperature. Figure 10 shows the linear regression of the adsorption kinetics for both the first-order and second-order models. The coefficient of determination (R^2) values for the pseudo-first-order model were 0.968, 0.839, and 0.840 for the 1:1, 1:2, and 2:1 ratios, respectively. In comparison, the R^2 values for the pseudo-second-order model were higher, at 1, 0.999, and 1, respectively, indicating that the pseudo-second-order model provides a better fit for the adsorption process across all three CaO/biochar ratios.

The higher R^2 values for the pseudo-second-order model suggest that the phosphate adsorption process is better described by this model, which assumes that chemical adsorption controls the process. This type of adsorption involves electron exchange or sharing between the adsorbent and adsorbate, potentially forming new compounds [33]. This finding illustrates that chemisorption is the dominant mechanism during phosphate adsorption on CaO/biochar, where the calcium in the eggshell chemically interacts with PO_4^{3-} [12].

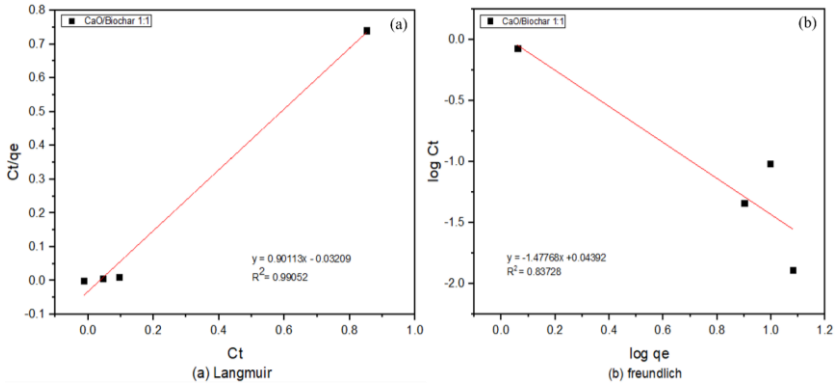

Figure 9. (a) Langmuir adsorption isotherm and (b) Freundlich adsorption isotherm of CaO/biochar

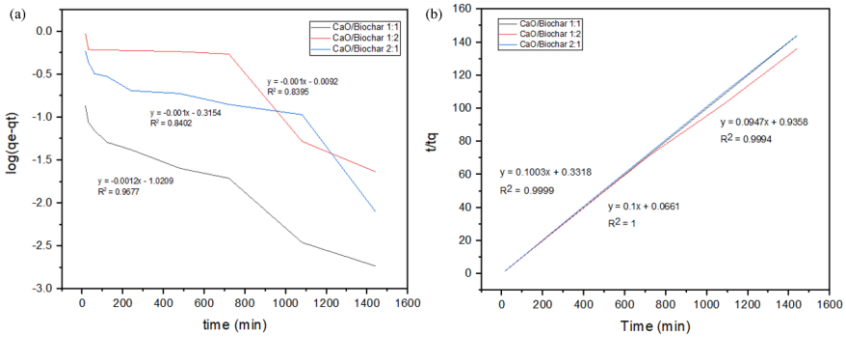

Figure 10. (a) linear regression of pseudo first order and (b) pseudo-second order adsorption kinetics of CaO/biochar

3.7. Synthesis of Binding Gel from CaO/biochar 1:2 and Ferrihydrite

The DGT device includes a binding gel that acts as an adsorbent, quickly and irreversibly adsorbing dissolved species, and a diffusive gel layer that allows dissolved species to pass through. The preparation of the diffusive gel and binding gel is based on a free radical polymerization reaction, using acrylamide as the monomer, N, N'-methylene bisacrylamide as the cross-linker, ammonium persulfate as the initiator, and TEMED as the catalyst, as described by Pato [34]. This study modified the binding gel using CaO/biochar material and ferrihydrite binding gel as a comparative binding agent [34].

As shown in Figure 11, the FTIR spectra of the diffusive gel, CaO/biochar binding gel, and ferrihydrite binding gel exhibit several peaks. FTIR characterization was performed to ensure that the acrylamide polymer was successfully synthesized. The peak at a wavenumber of 3335 cm^{-1} and 1631 cm^{-1} indicates the presence of O-H groups in ferrihydrite, as Russell [35] observed. At a wavenumber of 1386 cm^{-1}, there is a Fe-O, which is characteristic of ferrihydrite adsorption, consistent with the study by Pereira *et al.* [36]. The CaO groups in the FTIR spectrum of the CaO/biochar binding gel are shown at wavenumbers of ~834 cm^{-1} [13]. Two peaks at a wavenumber of ~3600 cm^{-1} for the diffusive gel sample are characteristic of amine stretching (−NH).

The peak at a wavenumber of 1114 cm^{-1} for the diffusive gel sample indicates aliphatic amine (C−N) adsorption, typically found in the 1250–1020 cm^{-1} wavenumber range. The functional groups present are the main functional groups of the acrylamide polymer, confirming that the acrylamide polymer was successfully synthesized. The functional groups observed in the diffusive gel, CaO/biochar gel, and ferrihydrite gel do not differ significantly, indicating no structural change in the polymer due to CaO/biochar and ferrihydrite. This data also suggests that the interactions between CaO/biochar, ferrihydrite, and acrylamide polymer are physical [37].

3.8. Diffusive Gradients in Thin Film Applications

3.8.1. Effect of Deployment Time Variation on Adsorption in CaO/biochar and Ferrihydrite Binding Gels

Figure 12 illustrates that the C_{DGT} values, which represent the concentration of phosphate adsorbed by the binding gel, are consistently higher for the CaO/biochar binding gel compared to the ferrihydrite binding gel across all deployment times (2, 4, 8, 12, and 24 hours). This trend highlights the better-than-phosphate adsorption capacity of CaO/biochar, attributed to its modification with calcium oxide (CaO), which enhances adsorption efficiency through ion exchange and surface complexation. The porous structure of CaO/biochar allows phosphate ions to replace hydroxyl (OH^-) or water (H_2O) groups on the biochar surface, forming stable phosphate complexes. In contrast, although effective, Ferrihydrite demonstrates lower adsorption capacity due to its reliance on weaker binding mechanisms such as electrostatic attraction or hydrogen bonding, resulting in significantly lower C_{DGT} values.

After 24 hours, ferrihydrite reaches a maximum of 2.5959 mg/L, whereas CaO/biochar achieves 10.1727 mg/L, nearly four times higher. This disparity underscores the effectiveness of CaO/biochar in enhancing phosphate adsorption. The findings align with diffusion theory, confirming that phosphate adsorption

is governed by ion diffusion to the binding gel surface [38, 39]. Moreover, Wang *et al.* [15] support this conclusion, demonstrating that calcium-decorated biochar has a high phosphate adsorption capacity of up to 314.22 mg/g, driven by the formation of hydroxylapatite ($Ca_5(PO_4)_3(OH)$) crystals. This suggests that CaO/biochar-based DGT devices are not only better than efficient but also better than for field applications, offering reliable and accurate phosphate measurement without requiring complex calibration processes.

3.8.2. Effect of Phosphate Concentration Variation on Adsorption in CaO/biochar and Ferrihydrite Binding Gels

As shown in Figure 13, the research results indicate that phosphate adsorption increases with the initial phosphate solution concentration due to the availability of active sites on the CaO/biochar and ferrihydrite binding gels, which serve as adsorbents. These sites provide locations where phosphate molecules can bind. At higher phosphate concentrations, more molecules are available in the solution, increasing the likelihood of phosphate molecules attaching to the adsorbent's active sites. As a result, higher initial concentrations lead to more phosphate being adsorbed. At lower concentrations, most active sites are quickly occupied, resulting in high adsorption efficiency. However, at higher concentrations, although the amount of adsorbed phosphate increases, the total capacity of the adsorbent approaches its maximum, and the efficiency per unit may decrease as the active sites become saturated.

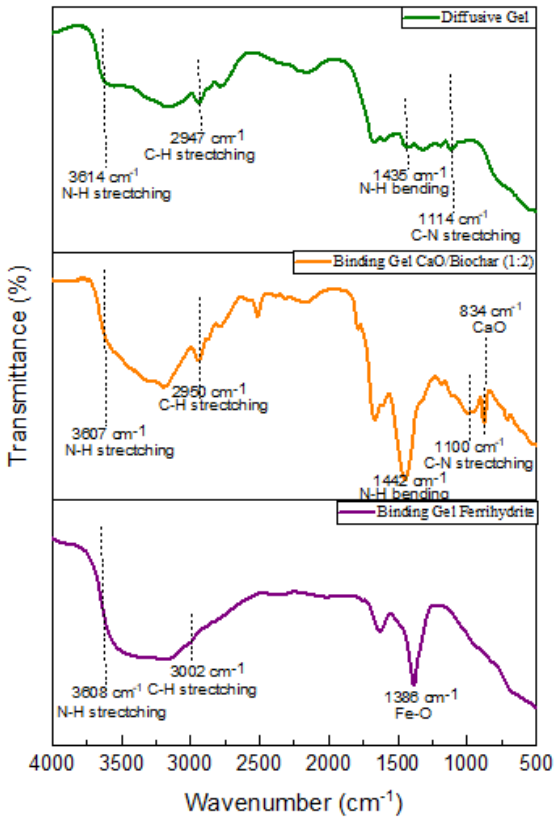

Figure 11. FTIR spectra of diffusive gel, CaO/biochar binding gel, and ferrihydrite

This experiment demonstrates that CaO/biochar and ferrihydrite binding gels effectively adsorb phosphate across various concentrations, with optimal C_{DGT} values at a 10 mg/L solution concentration of 9.13207 mg/L for CaO/biochar and 2.5471 mg/L for ferrihydrite binding gels. The maximum adsorption capacity is determined by the number of available active sites, which can become saturated at very high phosphate concentrations, leading to a relative decrease in adsorption efficiency. This study provides valuable insight into the maximum capacity of these adsorbents and identifies optimal conditions for using DGT devices to measure phosphate concentrations in different environments [40].

3.8.3. Effect of Phosphate Solution pH Variation on Adsorption in CaO/biochar and Ferrihydrite Binding Gels

pH levels play a significant role in determining phosphate measurements as they affect the chemical forms of phosphate, its solubility, and its interaction with the binding gel used in the measurement process. At low pH values, phosphate predominantly exists as $H_2PO_4^-$, while at higher pH levels, it transitions to hydrogen phosphate (HPO_4^{2-}) or phosphate (PO_4^{3-}). These forms exhibit different affinities for the binding gel, affecting how much phosphate is captured and thereby impacting measurement results. For example, as shown in Figure 14, the phosphate concentration measured by DGT varies with pH. The CaO/biochar binding gel achieves its highest phosphate adsorption of 4.953 mg/L at an optimal pH of 5, while the ferrihydrite binding gel reaches its peak adsorption of 1.3737 mg/L at an optimal pH of 3.

The optimal pH for phosphate adsorption is closely linked to the surface charge characteristics of each material. For CaO/biochar, the optimal pH of 5 aligns with its point of zero charge (pH_{pzc}), which is approximately 5.36, as indicated by recent studies [13]. At pH levels below this pH_{pzc}, the surface of CaO/biochar becomes positively charged due to the excess hydrogen ions (H^+) in the solution. This positive charge enhances the electrostatic attraction between the CaO/biochar surface and the negatively charged phosphate ions ($H_2PO_4^-$), thereby increasing phosphate adsorption.

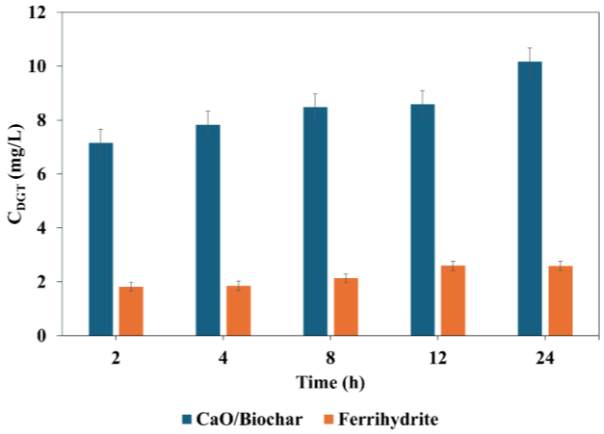

Figure 12. C_{DGT} value at various deployment times on the adsorption of CaO/biochar and ferrihydrite binding gel

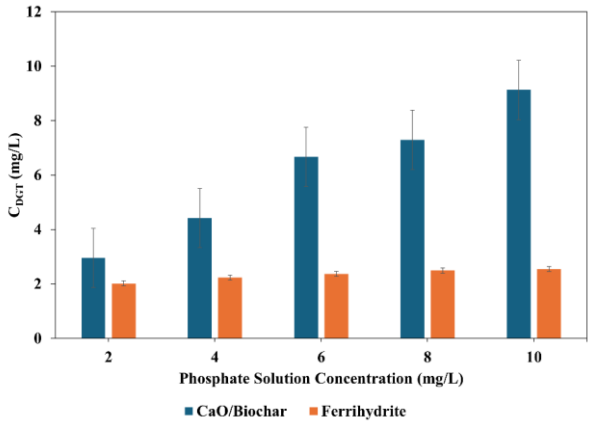

Figure 13. C_{DGT} value at various phosphate concentrations on the adsorption of CaO/biochar and ferrihydrite binding gel

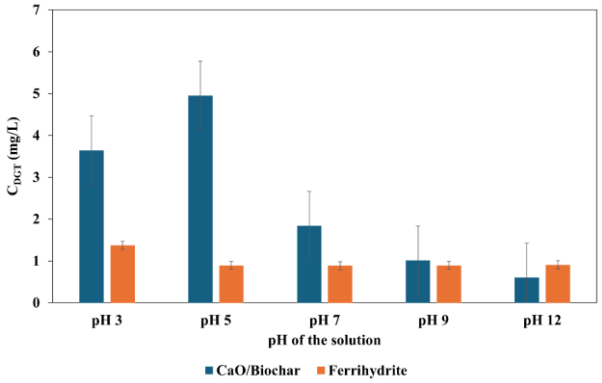

Figure 14. C_{DGT} value in varying pH of phosphate solution on the adsorption of CaO/biochar and ferrihydrite binding gel

Additionally, the presence of calcium ions (Ca^{2+}) in CaO/biochar facilitates the formation of stable phosphate complexes, such as hydroxyapatite ($Ca_5(PO_4)_3OH$), which further enhances adsorption efficiency. Conversely, for ferrihydrite, the optimal pH of 3 results in a highly protonated surface, generating a strong positive charge due to the high concentration of hydrogen ions. This protonation increases the electrostatic attraction to negatively charged phosphate ions, particularly $H_2PO_4^-$, leading to effective phosphate binding through electrostatic interactions and ligand exchange processes.

As the pH rises above these optimal values, the surface charge of both materials becomes less positive, reducing their adsorption efficiency. Thus, the optimal pH values for phosphate adsorption reflect each material's ability to attract and bind phosphate ions under different pH conditions, driven by their surface charge properties and chemical interactions. The efficiency of phosphate adsorption on these gels is influenced by pH because, at higher pH levels, the presence of OH^- ions weakens the ligand exchange, making phosphate binding less effective. Conversely, at lower pH levels, the gel surface becomes more positively charged, which enhances phosphate binding. This is why phosphate concentrations measured at lower pH are higher than those at higher pH [38].

4. Conclusion

In conclusion, this research demonstrates that CaO/biochar was effectively synthesized through ball milling and pyrolysis techniques using different mass ratios (1:1, 1:2, and 2:1) of eggshells and rice straw. Characterization methods such as FTIR, XRD, and surface area analysis confirmed the successful creation of the CaO/biochar composite. While the phosphate adsorption capacities across the different ratios were similar, the CaO/biochar (1:2) ratio showed the highest adsorption capacity. The study found that phosphate adsorption was significantly enhanced at pH 12 for all ratios, following the Langmuir adsorption isotherm and pseudo second-order kinetics. FTIR spectrum analysis validated the synthesis of the diffusive and binding gels, indicating that the interactions between CaO/biochar, ferrihydrite, and acrylamide polymer are primarily physical with no major structural changes. Additionally, the CaO/biochar binding gel proved to be a better material than the ferrihydrite binding gel for phosphate adsorption, achieving C_{DGT} values of 10.1727 mg/L and 2.5959 mg/L, respectively, at pH 5 and 3 with a 10 mg/L phosphate concentration. These results highlight the potential of CaO/biochar as a better material for phosphate removal applications.

References

[1] Nora Listantia Listantia, Analisis Kandungan Fosfat PO_4^{3-}- Dalam Air Sungai Secara Spektrofotometri Dengan Metode Biru-Molibdat, *SainsTech Innovation Journal*, 3, 1, (2020), 59-65 https://doi.org/10.37824/sij.v3i1.2020.171

[2] James Cooper, Rachel Lombardi, David Boardman, Cynthia Carliell-Marquet, The future distribution and production of global phosphate rock reserves, *Resources, Conservation and Recycling*, 57, (2011), 78-86 https://doi.org/10.1016/j.resconrec.2011.09.009

[3] Stefan Wan, Shengsen Wang, Yuncong Li, Bin Gao, Functionalizing biochar with Mg–Al and Mg–Fe layered double hydroxides for removal of phosphate from aqueous solutions, *Journal of Industrial and Engineering Chemistry*, 47, (2017), 246-253 https://doi.org/10.1016/j.jiec.2016.11.039

[4] Sónia G. Barbosa, Luciana Peixoto, Brendo Meulman, Maria Madalena Alves, Maria Alcina Pereira, A design of experiments to assess phosphorous removal and crystal properties in struvite precipitation of source separated urine using different Mg sources, *Chemical Engineering Journal*, 298, (2016), 146-153 https://doi.org/10.1016/j.cej.2016.03.148

[5] Yingyu Law, Rasmus Hansen Kirkegaard, Angel Anisa Cokro, Xianghui Liu, Krithika Arumugam, Chao Xie, Mikkel Stokholm-Bjerregaard, Daniela I. Drautz-Moses, Per Halkjær Nielsen, Stefan Wuertz, Rohan B. H. Williams, Integrative microbial community analysis reveals full-scale enhanced biological phosphorus removal under tropical conditions, *Scientific Reports*, 6, (2016), 25719 https://doi.org/10.1038/srep25719

[6] Ronghua Li, Jim J. Wang, Baoyue Zhou, Mukesh Kumar Awasthi, Amjad Ali, Zengqiang Zhang, Altaf Hussain Lahori, Amanullah Mahar, Recovery of phosphate from aqueous solution by magnesium oxide decorated magnetic biochar and its potential

as phosphate-based fertilizer substitute, *Bioresource Technology*, 215, (2016), 209-214 https://doi.org/10.1016/j.biortech.2016.02.125

[7] Deepak Yadav, Meghna Kapur, Pradeep Kumar, Monoj Kumar Mondal, Adsorptive removal of phosphate from aqueous solution using rice husk and fruit juice residue, *Process Safety and Environmental Protection*, 94, (2015), 402-409 https://doi.org/10.1016/j.psep.2014.09.005

[8] Anushka Upamali Rajapaksha, Season S. Chen, Daniel C. W. Tsang, Ming Zhang, Meththika Vithanage, Sanchita Mandal, Bin Gao, Nanthi S. Bolan, Yong Sik Ok, Engineered/designer biochar for contaminant removal/immobilization from soil and water: Potential and implication of biochar modification, *Chemosphere*, 148, (2016), 276-291 https://doi.org/10.1016/j.chemosphere.2016.01.043

[9] Hao Zhang, William Davison, Diffusional characteristics of hydrogels used in DGT and DET techniques, *Analytica Chimica Acta*, 398, 2, (1999), 329-340 https://doi.org/10.1016/S0003-2670(99)00458-4

[10] Asep Saefumillah, Amalia Ekaputri Hidayat, Studi Metode Diffusive Gradient In Thin Film dengan Binding Gel Titanium Dioksida-Chelex untuk Penyerapan Logam Besi (II) dan Fosfat Secara Simultan, *Jurnal Kimia VALENSI*, 3, 2, (2017), 134-141 https://doi.org/10.15408/jkv.v0i0.6078

[11] Chang Yoon Jeong, Jim J. Wang, Syam K. Dodla, Thomas L. Eberhardt, Les Groom, Effect of Biochar Amendment on Tylosin Adsorption–Desorption and Transport in Two Different Soils, *Journal of Environmental Quality*, 41, 4, (2012), 1185-1192 https://doi.org/10.2134/jeq2011.0166

[12] Evangelia Panagiotou, Nasia Kafa, Loukas Koutsokeras, Panayiotis Kouis, Petros Nikolaou, Georgios Constantinides, Ioannis Vyrides, Turning calcined waste egg shells and wastewater to Brushite: Phosphorus adsorption from aqua media and anaerobic sludge leach water, *Journal of Cleaner Production*, 178, (2018), 419-428 https://doi.org/10.1016/j.jclepro.2018.01.014

[13] Xiaoning Liu, Feng Shen, Xinhua Qi, Adsorption recovery of phosphate from aqueous solution by CaO-biochar composites prepared from eggshell and rice straw, *Science of The Total Environment*, 666, (2019), 694-702 https://doi.org/10.1016/j.scitotenv.2019.02.227

[14] Christopher Warwick, Antonio Guerreiro, Ana Soares, Sensing and analysis of soluble phosphates in environmental samples: A review, *Biosensors and Bioelectronics*, 41, (2013), 1-11 https://doi.org/10.1016/j.bios.2012.07.012

[15] Shengdan Wang, Lingjun Kong, Jianyou Long, Minhua Su, Zenghui Diao, Xiangyang Chang, Diyun Chen, Gang Song, Kaimin Shih, Adsorption of phosphorus by calcium-flour biochar: Isotherm, kinetic and transformation studies, *Chemosphere*, 195, (2018), 666-672 https://doi.org/10.1016/j.chemosphere.2017.12.101

[16] Asep Saefumillah, Dhania Dwi Aprianti, Iman Abdullah, Inna Husna, Modifikasi Lapisan Difusi dengan Pengikat Silang N, N'Metilenbisakrilamida (MBA) pada Sistem DGT Berbasis Gel dengan Adsorben TiO_2 untuk Penentuan Konsentrasi Fosfat di Lingkungan Akuatik, *Sainsmat: Jurnal Ilmiah Ilmu Pengetahuan Alam*, 2, 2, (2013), 173-184

[17] Arpana Agrawal, Gyu-Chul Yi, Chapter Two - Sample pretreatment with graphene materials, in: C.M. Hussain (Ed.) *Comprehensive Analytical Chemistry*, Elsevier, 2020, https://doi.org/10.1016/bs.coac.2020.08.012

[18] Vladislav A. Sadykov, Natalia V. Mezentseva, Lyudmila N. Bobrova, Oleg L. Smorygo, Nikita F. Eremeev, Yulia E. Fedorova, Yulia N. Bespalko, Pavel I. Skriabin, Alexey V. Krasnov, Anton I. Lukashevich, Tamara A. Krieger, Ekaterina M. Sadovskaya, Vladimir D. Belyaev, Alexander N. Shmakov, Zakhar S. Vinokurov, Vladimir A. Bolotov, Yuri Yu Tanashev, Mikhail V. Korobeynikov, Mikhail A. Mikhailenko, Chapter 12 - Advanced Materials for Solid Oxide Fuel Cells and Membrane Catalytic Reactors, in: V.A. Sadykov (Ed.) *Advanced Nanomaterials for Catalysis and Energy*, Elsevier, 2019, https://doi.org/10.1016/B978-0-12-814807-5.00012-7

[19] Maribel S. Tizo, Lou Andre V. Blanco, Andrian Cris Q. Cagas, Buenos Rangel B. Dela Cruz, Jimrey C. Encoy, Jemalyn V. Gunting, Renato O. Arazo, Val Irvin F. Mabayo, Efficiency of calcium carbonate from eggshells as an adsorbent for cadmium removal in aqueous solution, *Sustainable Environment Research*, 28, 6, (2018), 326-332 https://doi.org/10.1016/j.serj.2018.09.002

[20] Xin Huang, Jing-Pei Cao, Xiao-Yan Zhao, Jing-Xian Wang, Xing Fan, Yun-Peng Zhao, Xian-Yong Wei, Pyrolysis kinetics of soybean straw using thermogravimetric analysis, *Fuel*, 169, (2016), 93-98 https://doi.org/10.1016/j.fuel.2015.12.011

[21] Lennart Bäck, Melanie Josefsson, Lennart Strömquist, Land capability, recreational land-use and conservation strategies in a sensitive mountain environment. A method study from the Kiruna Mountains, Sweden, in: *UNGI rapport*, Uppsala University, 1989,

[22] Yuehui Jia, Shengli Shi, Jie Liu, Shiming Su, Qiong Liang, Xibai Zeng, Tingshu Li, Study of the Effect of Pyrolysis Temperature on the Cd^{2+} Adsorption Characteristics of Biochar, *Applied Sciences*, 8, 7, (2018), 1019 https://doi.org/10.3390/app8071019

[23] Rudy Syah Putra, Arida Liyanita, Nadia Arifah, Erlina Puspitasari, Sawaludin, Muhammad N. Hizam, Enhanced Electro-Catalytic Process on the Synthesis of FAME Using CaO from Eggshell, *Energy Procedia*, 105, (2017), 289-296 https://doi.org/10.1016/j.egypro.2017.03.316

[24] Mariam Onize Usman, Godwin Aturagaba, Muhammad Ntale, George William Nyakairu, A review of adsorption techniques for removal of phosphates from wastewater, *Water Science and Technology*, 86, 12, (2022), 3113-3132 https://doi.org/10.2166/wst.2022.382

[25] Abbas Ibrahim Hussein, Zuryati Ab-Ghani, Ahmad Nazeer Che Mat, Nur Atikah Ab Ghani, Adam Husein, Ismail Ab. Rahman, Synthesis and Characterization of Spherical Calcium Carbonate Nanoparticles Derived from Cockle Shells, *Applied Sciences*, 10, 20, (2020), 7170 https://doi.org/10.3390/app10207170

[26] M. Cabrera-Penna, J. E. Rodríguez-Páez, Calcium oxyhydroxide ($CaO/Ca(OH)_2$) nanoparticles:

Synthesis, characterization and evaluation of their capacity to degrade glyphosate-based herbicides (GBH), *Advanced Powder Technology*, 32, 1, (2021), 237-253 https://doi.org/10.1016/j.apt.2020.12.007

[27] Ei Ei Khine, Daniel Koncz-Horvath, Ferenc Kristaly, Tibor Ferenczi, Gabor Karacs, Peter Baumli, George Kaptay, Synthesis and characterization of calcium oxide nanoparticles for CO_2 capture, *Journal of Nanoparticle Research*, 24, 7, (2022), 139 https://doi.org/10.1007/s11051-022-05518-z

[28] Siyu Xu, De Li, Haixin Guo, Haodong Lu, Mo Qiu, Jirui Yang, Feng Shen, Solvent-Free Synthesis of MgO-Modified Biochars for Phosphorus Removal from Wastewater, *International Journal of Environmental Research and Public Health*, 19, 13, (2022), 7770 https://doi.org/10.3390/ijerph19137770

[29] Hongbin Yin, Ye Yun, Yinlong Zhang, Chengxin Fan, Phosphate removal from wastewaters by a naturally occurring, calcium-rich sepiolite, *Journal of Hazardous Materials*, 198, (2011), 362-369 https://doi.org/10.1016/j.jhazmat.2011.10.072

[30] Lei Sun, Shungang Wan, Wensui Luo, Biochars prepared from anaerobic digestion residue, palm bark, and eucalyptus for adsorption of cationic methylene blue dye: Characterization, equilibrium, and kinetic studies, *Bioresource Technology*, 140, (2013), 406-413 https://doi.org/10.1016/j.biortech.2013.04.116

[31] Fazhi Xie, Fengchang Wu, Guijian Liu, Yunsong Mu, Chenglian Feng, Huanhua Wang, John P. Giesy, Removal of Phosphate from Eutrophic Lakes through Adsorption by in Situ Formation of Magnesium Hydroxide from Diatomite, *Environmental Science & Technology*, 48, 1, (2014), 582-590 https://doi.org/10.1021/es4037379

[32] Bin Wang, Fang Guo, Shi-Hui Dong, Huimin Zhao, Activation of silent biosynthetic gene clusters using transcription factor decoys, *Nature Chemical Biology*, 15, (2019), 111-114 https://doi.org/10.1038/s41589-018-0187-0

[33] Jacob Lalley, Changseok Han, Xuan Li, Dionysios D. Dionysiou, Mallikarjuna N. Nadagouda, Phosphate adsorption using modified iron oxide-based sorbents in lake water: Kinetics, equilibrium, and column tests, *Chemical Engineering Journal*, 284, (2016), 1386-1396 https://doi.org/10.1016/j.cej.2015.08.114

[34] M. D. Pato, The practice of quantitative gel electrophoresis: by A Chrambach. pp 265. VCH Publishers. Florida. 1985. $45 ISBN 0-89-573-064-2, *Biochemical Education*, 15, 1, (1987), 52 https://doi.org/10.1016/0307-4412(87)90170-1

[35] J. D. Russell, Infrared spectroscopy of ferrihydrite: evidence for the presence of structural hydroxyl groups, *Clay Minerals*, 14, 2, (1979), 109-114 https://doi.org/10.1180/claymin.1979.014.2.03

[36] Rodrigo C. Pereira, Pedro R. Anizelli, Eduardo Di Mauro, Daniel F. Valezi, Antonio Carlos S. da Costa, Cássia Thaïs B. V. Zaia, Dimas A. M. Zaia, The effect of pH and ionic strength on the adsorption of glyphosate onto ferrihydrite, *Geochemical Transactions*, 20, 1, (2019), 3 https://doi.org/10.1186/s12932-019-0063-1

[37] Ardina Purnama Tirta, Asep Saefumillah, Foliatini Foliatini, Herawati Herawati, The Study of Phosphate Release from Artificial Sediment into Water Body Using Diffusive Gradient in Thin Film (DGT) Device in Oxic Condition, *Indonesian Journal of Chemistry*, 20, 2, (2020), 395-403 https://doi.org/10.22146/ijc.43482

[38] Khairuddin, Ruslan, Nindya Andarini, Widyastuti Oktriviani, Meiva Toda'a, Van Hindersen Kaope, Study of Phosphate Adsorption Using Ferrihydrite With Diffusive Gradient in Thin Films Method, *IOP Conference Series: Earth and Environmental Science*, 1075, (2022), 012002 https://doi.org/10.1088/1755-1315/1075/1/012002

[39] Chaosheng Zhang, Shiming Ding, Di Xu, Ya Tang, Ming H. Wong, Bioavailability assessment of phosphorus and metals in soils and sediments: a review of diffusive gradients in thin films (DGT), *Environmental Monitoring and Assessment*, 186, 11, (2014), 7367-7378 https://doi.org/10.1007/s10661-014-3933-0

[40] Adva Zach-Maor, Raphael Semiat, Hilla Shemer, Adsorption–desorption mechanism of phosphate by immobilized nano-sized magnetite layer: Interface and bulk interactions, *Journal of Colloid and Interface Science*, 363, 2, (2011), 608-614 https://doi.org/10.1016/j.jcis.2011.07.062